Cancer Biol Med 2026. doi: 10.20892/j.issn.2095-3941.2026.0468

ORIGINAL ARTICLE

OPEN ACCESS

Effective anti-PD-1 therapy reduces neutrophil infiltration *via* T cell–macrophage chemokine axis in hepatocellular carcinoma

Jiahao Huang[1]*, Boyang Yi[1]*, Kuo Qi[2], Delin Ma[3], Feifei Sun[4], Bo Han[4], Yijie Zhao[5], Wuzhou Wan[6], Ning Zhang[1,6,7,8], Rong Liu[1,9]

[1]Translational Cancer Research Center, Peking University First Hospital, Beijing 100034, China; [2]Department of Orthopedics, Affiliated Zhongshan Hospital of Dalian University, Dalian 116001, China; [3]Department of Hepatobiliary Surgery, Peking University People's Hospital, Beijing 100044, China; [4]Department of Pathology, Peking University People's Hospital, Beijing 100044, China; [5]Department of Laboratory Animal Science, Peking University Health Science Center, Beijing 100191, China; [6]Yunnan Baiyao Group, Kunming 650504, China; [7]Frontiers Science Center for Cancer Integrative Omics, International Cancer Institute, Peking University Health Science Center, Beijing 100191, China; [8]Department of Cell Biology, Tianjin Medical University Cancer Institute & Hospital, National Clinical Research Center for Cancer, Tianjin 300060, China; [9]Southwest United Graduate School, Kunming 650092, China

ABSTRACT

Objective: Immune checkpoint inhibitor (ICI) therapies, such as anti-PD-1 treatment, have achieved great success in various cancers, including hepatocellular carcinoma. Tumor-infiltrating lymphocytes have major roles in the mechanism of action for ICIs, but numerous other components of the tumor microenvironment also contribute to the effectiveness of immunotherapy. However, little is known about the changes in the tumor microenvironment after ICI therapy, which may sustainably affect tumor progression.

Methods: Integrated single-cell RNA sequencing data were collected for hepatocellular carcinoma (HCC) patient samples and analyzed to characterize immune cell alterations within the tumor microenvironment. Three different orthotopic allograft HCC models were established for ICI therapy and microenvironment component detection by using flow cytometry and multiple ELISA assays. Transwell assays were combined with flow cytometry to evaluate neutrophil migration. *In vitro* coculture systems were employed to investigate communication between different cell types. Multiplex immunochemistry analysis was conducted for human clinical samples to confirm the findings.

Results: Our results indicate that neutrophil infiltration was significantly reduced after effective ICI therapy, but not in patients with failed immunotherapy. Mechanistically, we found that effective anti-PD-1 therapy activates T cells, which secrete interferon-γ and other cytokines that act on tumor-associated macrophages. This T cell–macrophage crosstalk suppresses tumor-associated neutrophil-related chemokines secreted by macrophages. Consequently, neutrophil infiltration into the tumor microenvironment is diminished.

Conclusion: Our findings show that immunotherapy reinvigorates T cells, but also remodels the myeloid compartment and reduces neutrophil recruitment, potentially alleviating neutrophil-mediated immunosuppression, thereby providing potential myeloid-targeted combinatorial strategies for improving checkpoint blockade responses.

KEYWORDS Hepatocellular carcinoma; immunotherapy; tumor-associated macrophage; tumor-associated neutrophil; tumor-infiltrating lymphocyte

Introduction

Hepatocellular carcinoma (HCC) is the most common primary malignancy of the liver and the third leading cause of cancer-related mortality worldwide[1]. The pathogenesis of HCC is linked to chronic liver injury, inflammation, and fibrosis, which create a profoundly immunosuppressive and tolerogenic tumor microenvironment (TME)[2]. HCC is mainly caused by hepatitis B virus, hepatitis C virus, chronic alcohol

*These authors contributed equally to this work.
Correspondence to: Ning Zhang and Rong Liu
E-mail: zhangning@bjmu.edu.cn and liurong@bjmu.edu.cn
ORCID ID: https://orcid.org/0000-0001-7182-0100 and https://orcid.org/0000-0001-6123-9152
Received June 7, 2026; accepted October 8, 2026;
published online November 4, 2026.
Available at www.cancerbiomed.org
©2026 The Authors. Creative Commons Attribution-NonCommercial 4.0 International License (CC BY-NC 4.0)

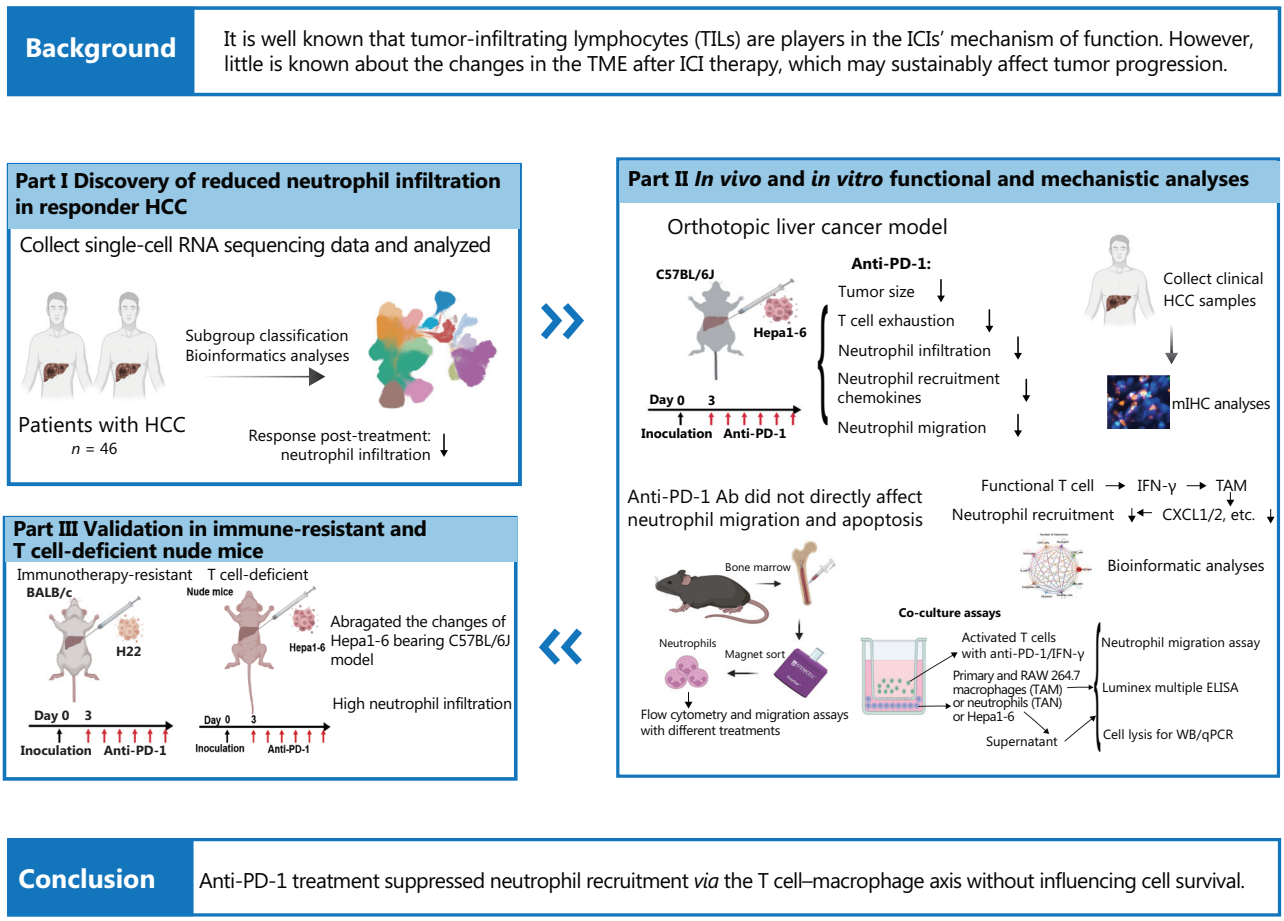

Study flowchart Schematic overview of the study design. **Part I:** Integrated single-cell transcriptomic analyses of patients with HCC to clarify the tumor microenvironment landscape, including the abundances of infiltrating immune cell subtypes. This part shows that the abundance of neutrophils decreased following anti-PD-1 immunotherapy in responders but not non-responders. **Part II:** *In vivo* and *in vitro* assays. Orthotopic liver cancer allografts were collected for flow cytometry, Luminex ELISA, and neutrophil migration assays. The tumor size, neutrophil infiltration, and neutrophil recruitment chemokines were reduced after anti-PD-1 treatment compared with immunoglobulin G (IgG) controls. Human clinical HCC samples were collected for multiplex immunohistochemistry analyses. Neutrophils were sorted from bone marrow in C57BL6/J mice for *in vitro* assays. Cell co-culture and cell –cell interaction analysis were performed to assess the mechanism involved. Anti-PD-1 treatment activated T cells to secrete interferon-γ, which further repressed macrophages that express a subset of chemokines, including CXCL1/5/2, involved in neutrophil recruitment. **Part III:** Immune checkpoint inhibitor-resistant H22 and T cell-deficient nude mice were used to validate the conclusions obtained in this study. The phenotypes characterized by neutrophil infiltration and neutrophil recruitment chemokines were not changed after anti-PD-1 treatment, with high neutrophil infiltration. ↓: decrease.

consumption, and metabolic dysfunction-associated steatohepatitis[3]. For decades, the treatment options for advanced HCC have been limited to multi-kinase inhibitors, such as sorafenib and lenvatinib, which provide only modest survival benefits[4,5]. The therapeutic landscape has been revolutionized by the introduction of the immune checkpoint blockade (ICB)[6]. The combination of atezolizumab (anti-PD-L1) and bevacizumab (anti-VEGF) has emerged as the global standard of care for first-line treatment[7]. However, despite this progress, primary and acquired resistance to ICB remains a significant hurdle, largely driven by the complex and dynamic nature of the HCC microenvironment, which contains immunosuppressive myeloid cells, tumor-associated neutrophils (TANs), fibroblasts, or exhausted effector T cells[8]. Understanding these resistance mechanisms and predictive biomarkers is critical for refining patient selection and developing next-generation combination strategies for treating this deadly disease.

The development of ICBs, especially those that target programmed cell death protein 1 (PD1) and its ligand PD-L1, has fundamentally improved the therapeutic landscape of medical oncology[9]. PD1, an inhibitory receptor, is mainly expressed on the surface of activated T cells. PD-L1 is the main ligand

of PD1 and is often upregulated in tumors and immune cells within the TME[10]. PD1 engaging with PDL1 leads to T cell exhaustion and enables immune evasion[11]. ICB therapies using monoclonal antibodies that block PD-1 (e.g., pembrolizumab and nivolumab) or its ligand PD-L1 (e.g., atezolizumab and durvalumab) disrupt this inhibitory interaction[12], effectively "releasing the brakes" on the immune system and reinvigorating exhausted tumor-infiltrating lymphocytes (TILs). However, ICB is still affected by significant challenges, where primary or acquired resistance limits its efficacy in a subset of patients, largely due to the complex and heterogeneous nature of the TME[13]. TILs have major roles in the mechanism of action for immune checkpoint inhibitor (ICIs), but the importance of the abundance of TILs and their pretreatment presence as predictors of the response to immunotherapy remains a controversial issue[14]. Previous studies mainly focused on changes in $CD8^+$ T cells after immunotherapies, without considering the changes and functional roles of other cells, especially myeloid cells within the TME[15,16], which may sustainably affect tumor progression.

Neutrophils are critical components of the immune system that act as first responders to infections. Recent research has highlighted the complex and dualistic role of TANs in cancer progression and therapeutic responses[17,18]. Neutrophils are highly plastic cells that can exhibit both antitumor and pro-tumor functions, and they are strongly influenced by cues within the TME[19]. Single-cell transcriptomic studies have demonstrated remarkable heterogeneity within the neutrophil compartment among tumor types[20-22]. Furthermore, neutrophil populations exhibit remarkable functional plasticity and can respond to local signals in the TME, participating in diverse processes, including angiogenesis, immune suppression, and antigen presentation[23-25]. Despite their diversity, we previously demonstrated that TANs promote tumor progression in an HCC mouse model[22], and a high density of neutrophils in the TME is frequently associated with poor prognosis and resistance to ICI therapies in solid tumors[26]. Retrospective studies also found that a high baseline neutrophil-to-lymphocyte ratio in the peripheral blood predicts a poor response and reduced survival in patients undergoing ICB[27]. However, despite their prognostic value, the underlying biological mechanisms involved remain largely unclear. Previous studies have focused on $CD8^+$ T cells and other immune cells in the TME[28], but the changes in TANs and their roles in the context of immunotherapy remain largely unexplored, although human single-cell immunotherapy data are available. Thus, in the present study, we comprehensively investigated the role of neutrophils in the response of HCC cells to anti-PD-1 immunotherapy. Neutrophil infiltration was significantly reduced in the TME following immunotherapy, and the T cell–macrophage axis was identified as an important mechanism for regulating neutrophil infiltration. Our findings suggest that dynamically monitoring the abundance of neutrophils during treatment may be used as an indicator of the response to immunotherapy.

Materials and methods

Mouse and orthotopic tumor models

Male C57BL/6J mice (8 weeks old), male BALB/c mice (8 weeks old), and male immunodeficient nude mice (8 weeks old) were obtained from the Department of Laboratory Animal Science, Peking University Health Science Center. All mice were maintained under specific pathogen-free conditions with a 12 h/12 h light/dark cycle and free access to food and water. All animal experiments were approved by the Institutional Animal Care and Use Committee of the Peking University and performed in accordance with the relevant guidelines and regulations (Approval No. PUIRB-LA2022626).

For orthotopic HCC models, mice were anesthetized with tribromoethanol. After disinfecting the skin with iodophor solution, a 1 cm incision was made along the medioventral line below the breastbone to expose the liver. Next, 50 μL of a mixture containing 1×10^6 Hepa1-6 cells or H22 cells mixed 9:1 with Matrigel matrix (Corning) was slowly injected into the liver in C57BL/6J mice and BALB/c mice, followed by abdominal closure. The abdomen was stitched in two layers and the mice were monitored until full recovery.

For anti-PD-1 blockade, mice were randomly assigned to treatment or control groups ($n = 6$). Anti-PD-1 antibody (BioXCell) or isotype control immunoglobulin G (IgG) (BioXCell) was administered intraperitoneally at a dose of 200 μg per mouse twice weekly. Treatment was initiated at four days post-tumor implantation. Tumor growth was monitored by measuring abdominal bulging and each mouse's status. The mice were euthanized at the experimental endpoint approximately 20 days after injection. Tumor tissues were harvested for flow cytometry and multiplex ELISA.

Patient sample collection

This study was approved by the Research Ethics Committee of Peking University First Hospital (Approval No. 2026R0091-0001). Written informed consent was obtained from each patient. Samples from patients with HCC who received immunotherapy between 2022–2026 were stratified according to treatment outcomes as responders partial response/complete response (PR/CR) and non-responders progressive disease/stable disease (PD/SD), and screened for this study.

Cell lines and culture conditions

The HCC cell line Hepa1-6 was purchased from ATCC. The murine cell line RAW 264.7 was a gift from Professor Han's laboratory (Peking University). Hep1-6 cells were cultured

in special Hep1-6 cell complete medium supplemented with 8% fetal bovine serum (FBS; Gibco) at 37°C in a humidified atmosphere containing 5% CO_2. Tumor cell supernatant (tumor-conditioned medium; TCM) was collected from confluent cultures after 48 h, centrifuged at 1,500 rpm for 10 min to remove any debris, and filtered through a 0.22 μm membrane. RAW 264.7 cells were maintained in Dulbecco's modified Eagle medium (DMEM; Gibco) supplemented with 10% FBS. All cell lines were routinely tested for mycoplasma contamination.

Flow cytometry analysis

Tumor tissues were minced and digested using a Tumor dissociation kit (Miltenyi Biotec) and gentleMACS™ Octo Dissociator with Heaters according to the manufacturer's instructions. The digested tissue was passed through a 70 μm cell strainer to obtain single-cell suspensions. Red blood cells were lysed in ACK lysis buffer. Single-cell suspensions were first stained with fixable viability stain 510 (FVS510) to exclude dead cells, before incubating with rat anti-mouse CD16/CD32 (BD, 2.4G2) (FcR blocker) monoclonal antibody, followed by surface staining at 4°C for 25 min. The following antibodies were used: anti-CD45 (BD, 30-F11, 1:100), anti-CD11b (BD, M1/70, 1:100), LY6G (BioLegend, 1:100), CD3 (BD, 500A2, 1:100), CD8 (BD, 53–6.7, 1:100), anti-CD4 (BioLegend, 1:100), anti-PD-1 (BD, 29F.1A12, 1:100), anti-TIM-3 (BioLegend, 1:100), anti-F4/80 (BD, 45–2,342, 1:100), anti-NK1.1 (BD, PK136, 1:100), and anti-CD86 (BD, GL1, 1:100). Flow cytometry analysis was performed using an Aurora spectral flow cytometer (Cytek Biosciences). At least 50,000 live $CD45^+$ cells were collected from each sample. Data were analyzed using FlowJo software (v10.8). The gating strategy used to identify the immune cell populations is shown in **Figure S2**.

Neutrophil and T cell isolation

Neutrophils were isolated from the bone marrow or tumors in tumor-bearing C57BL/6J mice. The femurs and tibiae were dissected, and the bone marrow was flushed with cold phosphate-buffered saline (PBS). Neutrophils were sorted by magnetic-activated cell sorting (MACS) using anti-Ly6G MicoBeads (BioLegend) or a mouse neutrophil negative selection kit (STEMCELL), according to the manufacturer's instructions. The purity and viability of cells were confirmed by flow cytometry.

For T cell isolation, spleens from tumor-bearing C57BL/6J mice were harvested and homogenized through a 70 μm cell strainer. T cells were sorted by negative selection using an EasySep™ Mouse T Cell Isolation Kit (STEMCELL) according to the manufacturer's instructions.

Primary bone marrow derived macrophages

Bone marrow cells were isolated from syngeneic C57BL/6J mice. Cell suspensions were filtered through a 70 μm cell strainer, followed by red blood cell lysis using ACK lysis buffer. After centrifugation, cells were cultured in complete DMEM supplemented with 20 ng/mL mouse M-CSF (TargetMol, TMPS-00102). After culture for 5 days, the primary macrophages exhibited cytoplasmic protrusions, and were harvested for designed assays.

Multiplex immunohistochemistry (mIHC) of clinical HCC samples

Clinical HCC tissue slides were deparaffinized with xylene and rehydrated using a graded series of ethanol solutions (100%, 95%, and 70%). Subsequently, antigens were retrieved by boiling the slides in citric acid solution for 15 min. Tissue slides were incubated with primary antibodies against CD66b (#305102, BioLegend), CD68 (#ZM0060, Zsbio), CD8 (#bsm-61078R, Bioss), and CXCL8 (#CST94407, CST) for 0.5 h at 37°C, before incubating with rabbit/mouse HRP-conjugated secondary antibody for 10 min at 37°C. An Alpha X 8-Color IHC Kit (#AXT38100031, Alpha X Bio) was used for visualization. After each staining cycle, heat-induced epitope retrieval was performed to remove all free antibodies, including primary and secondary antibodies. The nuclei in samples were counterstained with 4′,6-diamidino-2-phenylindole (DAPI) and mounted in mounting medium. Multispectral images were scanned with a ZEISS AXIOSCAN 7. Cells of interest were quantified using Halo (v.3.4; Indica Labs) or QuPath (v.0.2.0).

Apoptosis and necrosis assay

Neutrophils were seeded in 96-well U-bottom plates at 4×10^5 cells per well in 150 μL RPMI 1640 supplemented with 10% FBS. Cells were treated with anti-PD-1 antibody (10 μg/mL, BioXCell) or isotype control IgG (10 μg/mL, BioXCell). To generate model TANs, neutrophils were preincubated for 24 h with 50% (v/v) TCM derived from Hep1-6 cells.

After treatment, the cells were harvested, washed twice with PBS, and resuspended in 1× Annexin V binding buffer (BD Biosciences). The cells were stained with Annexin V-FITC (BD Biosciences) for 15 min at room temperature in the dark and washed twice with PBS. Propidium iodide (PI) was added before flow cytometric analysis. A CytoFLEX flow cytometer was used and at least 30,000 cells were acquired per sample. Data were analyzed using FlowJo software (v10.8). The percentage of late apoptotic cells ($Annexin\ V^+/PI^+$) was quantified.

Co-culture of T cells and macrophages for neutrophil migration and ELISA assay

The mouse macrophage cell line RAW 264.7 was induced to differentiate into tumor-associated macrophages (TAMs) by

pre-culturing with TCM. Sorted T cells were activated with anti-CD3 and anti-CD28 antibodies (BioLegend). TAM-like RAW 264.7 cells or other indicated cells were cultured in the lower chamber, and activated T cells were cultured in the upper chamber with a 0.4 μm pore membrane Transwell insert. Anti-PD-1 blocking antibody was added for the antibody intervention or isotype IgG control (BioXCell). Anti-interferon-γ (–IFN-γ) antibody (BioXCell) was added to neutralize the IFN-γ secreted from T cells. The cells were co-cultured for 24 h. The medium was collected from TAM-like RAW 264.7 or other indicated cells for neutrophil migration and multiple ELISA assays.

Neutrophil migration assay

Neutrophil migration was assessed using 24-well Transwell plates with 5 μm pore polycarbonate membranes (Corning), where 2.5×10^5 purified neutrophils were placed in the upper chamber in 150 μL serum-free RPMI 1640 medium, and the lower chamber contained 600 μL RPMI 1640 supplemented with 10% FBS. For the anti-PD-1 migration assay, neutrophils were treated with anti-PD-1 antibody or isotype IgG at 10 μg/mL. After incubating for 3.5 h at 37°C, neutrophils that migrated into the lower chamber were collected and counted using flow cytometry.

For the T cell-macrophage co-culture supernatant chemotaxis assay, the lower chamber of the Transwell plate was filled with TAM-like RAW 264.7 medium mixed 1:1 with fresh RPMI 1640 medium containing 10% FBS. All experiments were performed in triplicate and repeated at least three times.

To assess tumor lysate-mediated neutrophil migration, lysates from tumors treated with anti-PD-1 or IgG control were centrifuged, before harvesting and filtering the supernatants. The lower chamber of the Transwell plate was filled with filtered tumor lysate mixed 1:1 with 10% FBS supplemented RPMI 1640 medium.

Multiple ELISA assay

Cytokine concentrations were determined using a Bio-Plex Pro Mouse Chemokine 31-Plex Panel Kit (Bio-Rad) according to the manufacturer's protocol. First, capture antibodies precoupled to magnetic beads were added to the wells and washed with wash buffer. Subsequently, the samples were added and incubated with the coupled beads on a shaker for 30 min at 850 rpm and room temperature. After washing, biotinylated detection antibodies were added, before incubating for 30 min on a shaker at 850 rpm and room temperature to produce sandwich complexes. After several washes to remove unbound proteins, the final detection complex was formed by adding streptavidin-phycoerythrin conjugate and incubating for 10 min on a shaker at 850 rpm and room temperature. Finally, the samples were detected using a Synergy H1 plate reader, and the obtained data were processed and analyzed.

Fresh tumor masses from the tumor tissue samples were minced into small pieces and lysed for ELISA. For the T cell–macrophage co-culture system, supernatants from TAM-like RAW 264.7 were prepared as described above. A 50 μL aliquot of each supernatant was loaded per well.

RNA extraction, reverse transcription, and quantitative real-time PCR (qPCR)

Total RNA was extracted from the samples using TRIzol reagent (#15596026, Invitrogen), and the RNA concentration was measured with a Nanodrop system. Next, 1 μg RNA was reverse transcribed into cDNA using an RT reagent kit (#AU341, TransGen Biotech) according to the manufacturer's protocol. qPCR was performed using a QuantStudio 6 Flex system with SYBR Green qPCR SuperMix (#AQ631, TransGen Biotech). Three biological and three technical replicates were used for each treatment group. The primer sequences are shown in **Table S1**.

Western blotting

Whole cell protein was extracted from primary macrophages using RIPA buffer supplemented with phosphatase and protease inhibitors. Protein concentrations were determined by using the BCA assay. For each sample, 30 μg of protein was loaded for sodium dodecyl sulfate–polyacrylamide gel electrophoresis and then transferred to polyvinylidene fluoride membranes (0.45 μm). Membranes were blocked with 5% bovine serum albumin and incubated with primary anti-phosphorylated STAT1 (#9167S, CST) and anti-GAPDH (#ab181602, Abcam) antibodies, before incubating with horseradish peroxidase-linked secondary antibodies. Signals were detected using Amersham ImageQuant 800 Western blot imaging systems (Cytiva). GAPDH was used as the internal reference.

Single-cell RNA sequencing (scRNA-Seq) data collection, integration, and analysis

Publicly available scRNA-Seq data sets from patients with HCC who received immunotherapy were obtained from published articles[28-31]. The Gene Expression Omnibus database and associated accession numbers are indicated in the Data Availability section. All data sets were preprocessed using a standardized pipeline. Raw count matrices were loaded into R (version 4.x) and analyzed using the Seurat package (version 5.x). The quality of cells was assessed according to three metrics: (1) the number of total unique molecular identifier (UMI) counts per cell (library size) was below 30,000; (2) the number of detected genes was above 500 and below 6,000; and (3) the percentage of mitochondrial genes was below 50. Next, we used a cluster-level approach to remove potential doublet cells.

The scanpy (v.1.6) Python package was used to identify major cell types[32]. We regressed the effect of the percentage of mitochondrial genes and scaled each gene to unit variance. The dimensionality of each data set was reduced using Uniform Manifold Approximation and Projection for Dimension Reduction (UMAP). We first annotated the 15 major cell types identified in our data set based on well-known marker genes: *CD3D*, *CD8A*, *CD4*, *FOXP3*, *TRDC*, *NKG7*, *CD79A*, and *MS4A1* for the lymphoid lineage ($CD8^+$ T, conventional $CD4^+$ T, T regulatory, natural killer, and B cells); *CD14*, *CD16*, *CD68*, *CD163*, *CD1C*, *LAMP3*, *TPSAB1*, *CSF3R*, and *S100A8* for the myeloid lineage (macrophages, dendritic cells, and neutrophils); *VWF* and *COL1A1* for stromal cells (endothelial cells and fibroblasts); and *ALB* and *EPCAM* for epithelial cells. Epithelial cells comprising hepatocytes, cholangiocytes, and progenitor cells were analyzed using cluster analysis. Subclustering was performed for each major cell type to identify finer populations.

To visualize the expression of key chemokines and phenotypic genes among groups, we generated UMAP feature plots using the FeaturePlot function in Seurat, where each cell was colored according to the normalized expression level of a given gene. We extracted the average expression values per cell type and sample to quantitatively compare gene expression among different groups. The FeaturePlot, VlnPlot, and DotPlot functions in Seurat were used to visualize the gene expression patterns. All bioinformatics analyses were conducted in R (v4.3.1) with core dependencies, including Seurat (v5.0), ggplot2 (v3.4.4), and pheatmap (v1.0.12).

Cell–cell interaction analysis

To investigate cell–cell interactions among T cells and other cell types in the TME, we analyzed ligand–receptor (L–R) pairs using CellChatDB and CellphoneDB (v.2.1.7). Briefly, a log2-normalized count matrix was subsampled into 500 cells per cluster. Significant L–R pairs were identified after filtering for frequencies below 0.1% or above 2% among all cluster–cluster combinations. For each L–R pair, the total number of pairs was counted among clusters from the same cellular module. Cellular module-specific L–R pairs were then determined based on the enrichment score using Ro/e values (Ro/e >3).

Statistical analysis

Data were expressed as the mean ± standard deviation. Statistical analyses were performed using GraphPad software version 8.0.1. Comparisons between two groups were performed using two-tailed Student's *t*-tests. Statistically significant differences were accepted at $P < 0.05$. Significant differences: $^*P < 0.05$, $^{**}P < 0.01$, $^{***}P < 0.001$. NS, not significant. All data presented in the main figures are representative of at least three independent experiments.

Results

scRNA-Seq analyses elucidated neutrophil dynamics associated with the response to immunotherapy in patients with HCC

To explore how the TME was remodeled after effective or failed ICI therapy, we integrated four scRNA-Seq data sets containing 104 samples from 46 patients with HCC who received immunotherapy[28-31] and analyzed the composition of the TME. After reducing the data dimensionality (**Figure S1**), we successfully identified the major immune cell populations, including T cells, macrophages, and neutrophils (**Figure 1A**). To visualize the distributions of these populations according to the treatment and response context, the patients were stratified into four groups: responders before and after treatment, and non-responders before and after treatment. A clear shift in the UMAP landscape was found among the four groups (**Figure 1B**). Among T cells, IFN-γ expression was highest in responders after treatment, indicating that T cells were mostly reinvigorated in this group (**Figure 1C**). Interestingly, we also found a significant reduction in the abundance of neutrophils following anti-PD-1 immunotherapy in responders but not non-responders (**Figure 1D**).

Anti-PD-1 treatment suppressed tumor growth and reduced neutrophil infiltration

To validate this finding and evaluate the impact of ICB on the tumor immune microenvironment, we established an immunotherapy-sensitive Hepa1-6[33] orthotopic HCC mouse model with anti-PD-1 or IgG isotype controls (**Figure 2A**). As expected, PD-1 blockade significantly suppressed tumor growth compared with the control, confirming the therapeutic efficacy of this intervention in HCC (**Figure 2B**). To further evaluate changes in the composition of the TME, tumor-infiltrating immune cells were analyzed by flow cytometry. The gating strategy for flow cytometry analysis is shown in **Figure S2**. Consistent with the established mechanism of PD-1 therapy, we observed a marked reduction in $CD8^+$ T cell exhaustion, as indicated by the decreased expression of exhaustion markers PD-1 and TIM-3 in $CD8^+$ T cells in the anti-PD-1 group (**Figure 2C, D**), but the total $CD8^+$ T cell population remained unchanged. The frequencies of natural killer (NK) cells, $CD4^+$ T cells, and macrophages remained unchanged in these groups (**Figure 2E–G**). Strikingly, the amount of TANs was significantly reduced in the anti-PD-1-treated group (**Figure 2H**), which aligns with human data (**Figure 1D**). However, these changes were not observed in the ICI-resistant H22 allograft model (**Figure S3A–D**). It should be noted that the proportion of TANs in ICI-resistant H22 tumors, which accounted for approximately 50% of $CD45^+$ cells (**Figure S3C**), was much higher than that in Hepa1-6 tumors. In

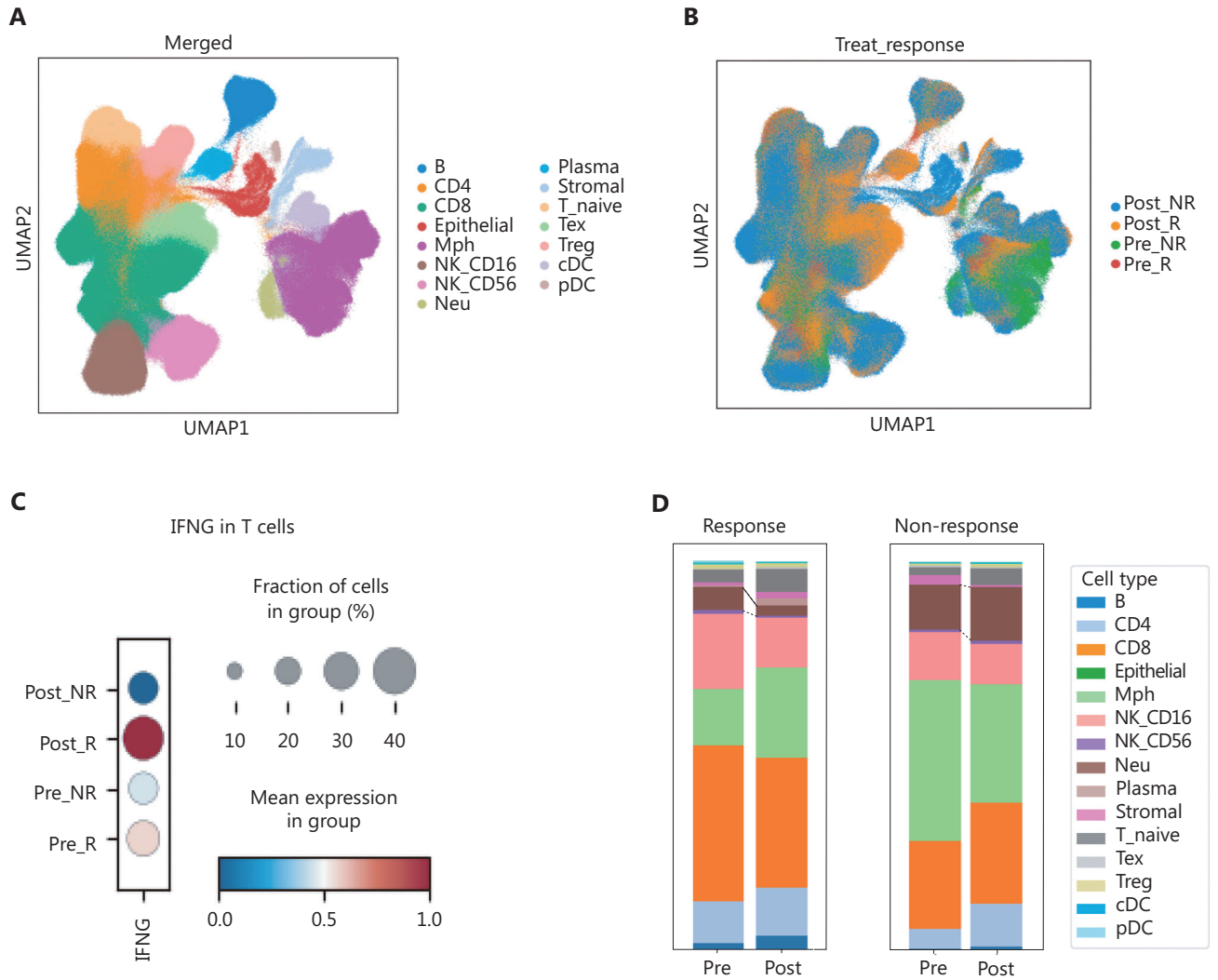

Figure 1 Tumor-associated neutrophil population decreased in immunotherapy-responsive patients with HCC. (A) Integrated single-cell atlas combining independent data sets. Dimensionality reduction (UMAP) and unsupervised clustering of cells allowed annotation based on marker genes (n = 104). (B) UMAP visualization of four patient groups: responders before treatment (pre_R), responders after treatment (post_R), non-responders before treatment (pre_NR), and non-responders after treatment (post_NR). (C) Dot plot showing the expression of interferon-γ in T cells among the four groups. (D) Fractions of different cell types in the TME among the four patient groups.

addition, tumor-infiltrating T cells were present at extremely low levels (about 8% of $CD45^+$ cells) (**Figure S3D**). These results suggest that high neutrophil infiltration contributes to an immune-suppression phenotype.

Anti-PD-1 treatment reduced neutrophil motility and did not directly affect neutrophil migration and apoptosis

To determine how the TAN population was regulated by PD-1 blockade in the TME, we then performed *in vitro* assays to evaluate the direct effects of PD-1 blockade on neutrophils (**Figure 3A**). The purity and viability of primary neutrophils isolated from the bone marrow of C57BL/6J mice were assessed by flow cytometry, which showed that the sorting efficiency was >95%, and the isolation procedure did not impair the viability of neutrophils (**Figure S4**). To determine whether anti-PD-1 treatment directly induced neutrophil cell death, purified neutrophils were treated with anti-PD-1 for Annexin V/PI apoptosis assays using flow cytometry. In addition, neutrophils were cultured in the presence of Hepa1-6 culture supernatants prior to anti-PD-1 treatment. The results showed that the ratio of apoptotic neutrophils relative to TCM-induced TANs did not change significantly (**Figure 3B**), indicating that the reduction in neutrophil infiltration observed *in vivo* was

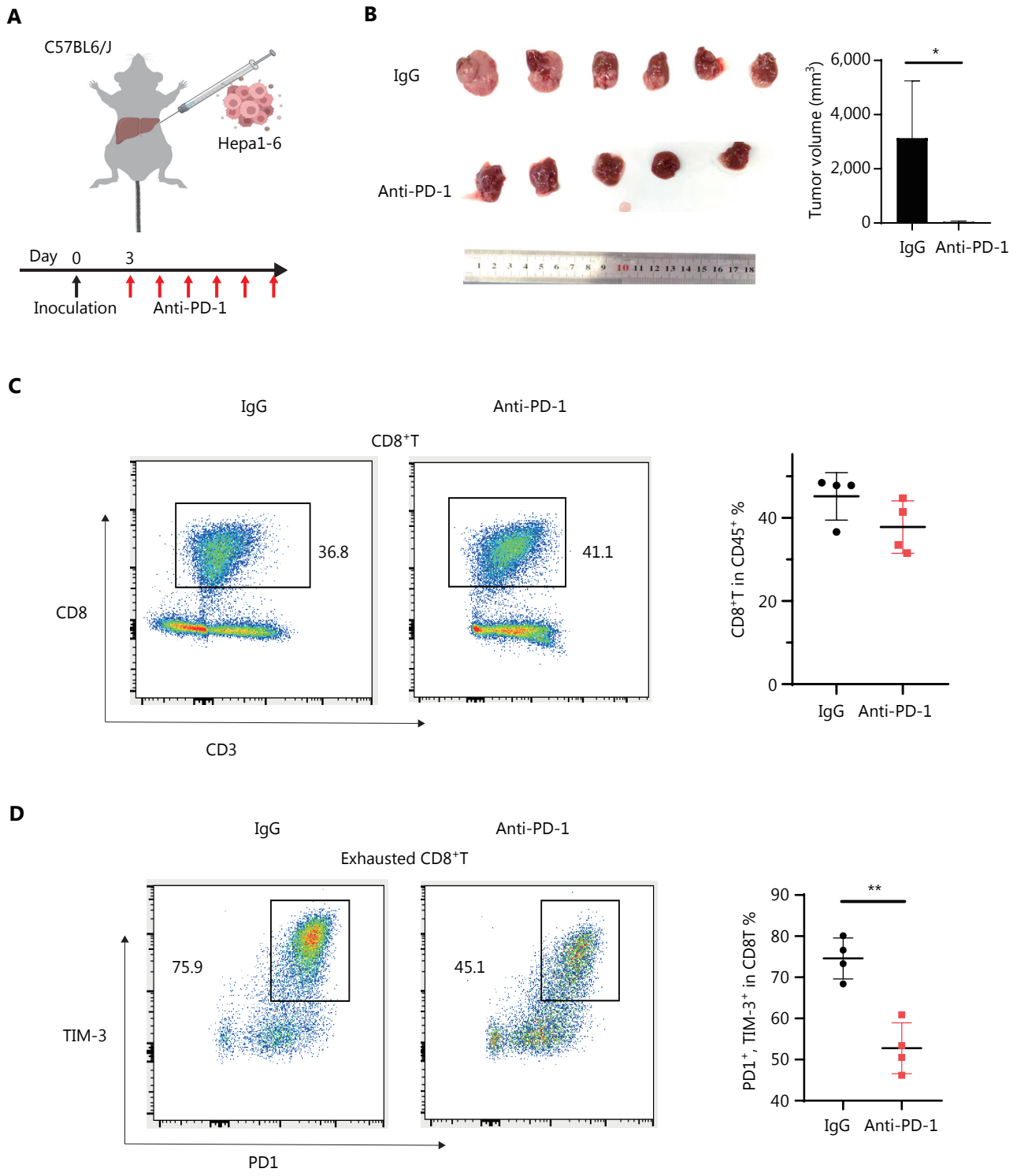

Figure 2 Continued

probably not due to the direct cytotoxic effects of the antibody. We also examined whether anti-PD-1 treatment directly affected neutrophil migration (**Figure 3C**). Under treatment with the anti-PD-1 antibody, the number of migrating neutrophils did not decrease significantly compared with those in the IgG or PBS treatment groups (**Figure 3C**). However,

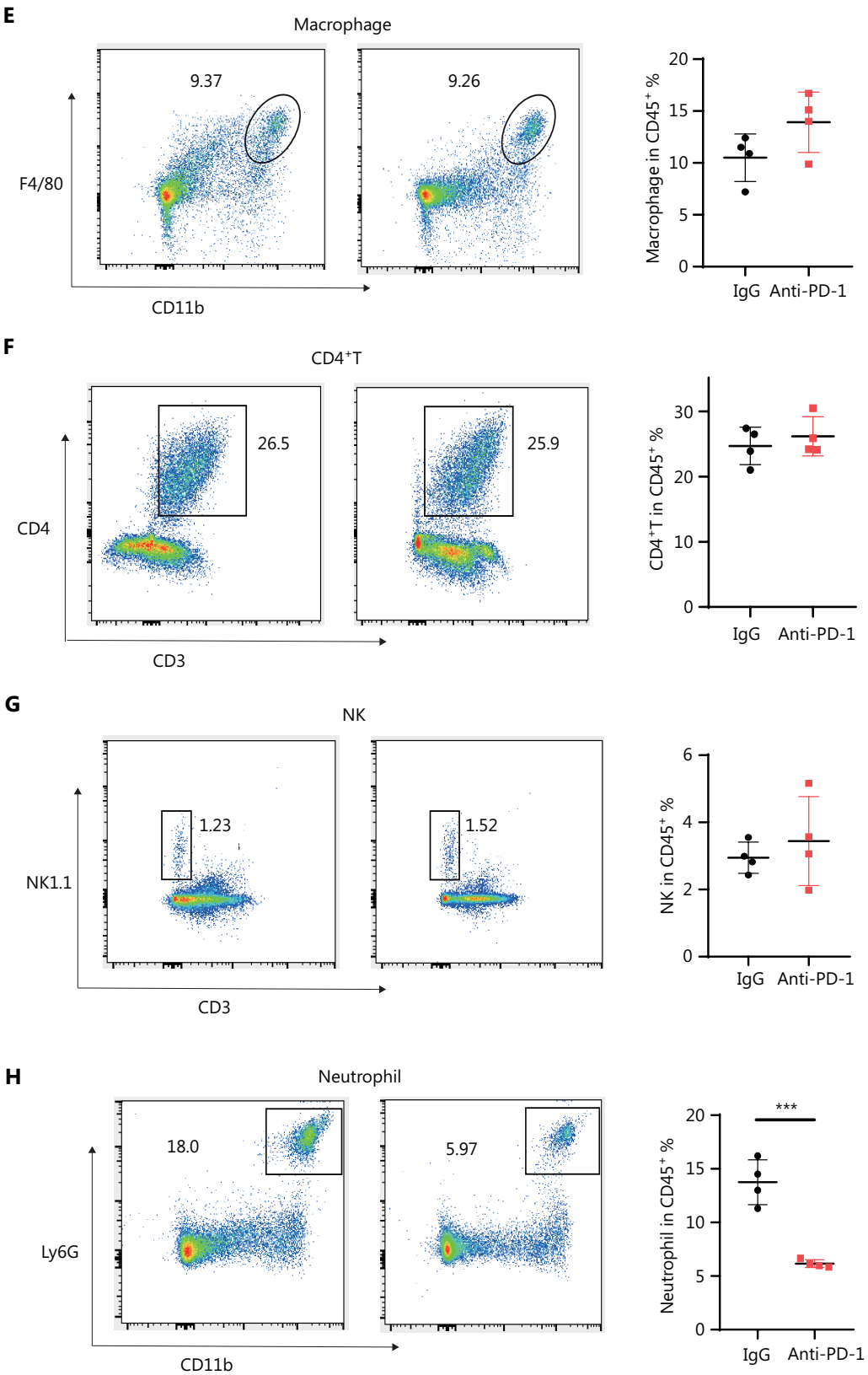

Figure 2 Effective anti-PD-1 therapy reduced infiltration of neutrophils in the TME. (A) Hepa1-6 cells (1×10^6 cells/point) were orthotopically implanted into the liver of C57BL/6J mice, before administering anti-PD-1 antibody (n = 5) or isotype control IgG (n = 6) twice each week. (B)

Anti-PD-1 immunotherapy suppressed Hepa1-6 cell growth *in vivo*. Quantification of tumor sizes at the endpoint shown on the right. (C–H) Flow cytometric analysis of TME cells in orthotopic HCC tumors. Percentages of tumor infiltrating $CD8^+$ T cells (C), exhausted $CD8^+$ T cells (D), tumor-associated macrophages (E), tumor infiltrating $CD4^+$ T cells (F), natural killer (NK) cells (G), and tumor-associated neutrophils in $CD45^+$ cells (H). $^*P < 0.05$, $^{**}P < 0.01$, $^{***}P < 0.001$, unpaired two-tailed Student's *t*-test. All data represent the mean ± standard error of the mean.

when the chemotactic medium was replaced with the lysate (1:1 dilution with RPMI 1640 medium) from anti-PD-1 or IgG control-treated tumors, the migration of neutrophils was significantly inhibited in the presence of tumor lysate from the anti-PD-1 group compared with the IgG group (**Figure 3D**), suggesting that components of the TME other than T cells are involved in regulating the effect of anti-PD-1 on neutrophil infiltration into tumors.

Furthermore, anti-PD-1 antibodies directly bind to the receptor PD-1 in order to function, so we compared the expression of PD-1 in neutrophils and $CD8^+$ T cells. Flow cytometry showed that neutrophils from the bone marrow, peripheral blood, or tumors did not express PD-1. PD-1 expression was low in TANs and far lower than the expression level in $CD8^+$ T cells, which are classical PD-1 expressers (**Figure 3E**). In summary, these results support the hypothesis that the reduction in the abundance of neutrophils after anti-PD-1 treatment is probably due to decreased infiltration of the tumor mass caused by other components of the TME.

Macrophages were the primary source of neutrophil-related chemokines and regulated by T cells

Chemokines are critical for recruiting neutrophils to solid tumors, so we collected tumor lysates from orthotopic Hepa1-6 allografts treated with anti-PD-1 or IgG for multiple Luminex ELISA. The ELISA panel showed that the levels of neutrophil recruitment-related chemokines were significantly decreased under anti-PD-1 treatment (**Figure 4A**), especially key neutrophil chemoattractants, including CXCL1 and CXCL5, which were significantly lower in the anti-PD-1 group (**Figure 4B**). In addition, the levels of several inflammatory cytokines that attract neutrophils[34,35] were significantly reduced under anti-PD-1 treatment (**Figure 4C**). These results indicate that the TME of anti-PD-1 treated tumors is less chemotactic, consistent with reduced neutrophil infiltration in the TME after effective immunotherapy.

We used human single-cell data to investigate the origins of these neutrophil-related chemokines in the TME of HCC. Visualizing the integrated human single-cell atlas showed that the expression levels of neutrophil-related chemokines, including CXCL8/1/2, were higher in macrophages compared with other cell populations (**Figure 4D**). Feature mapping further confirmed that CXCL8, which is one of the most important neutrophil-related chemokines, was predominantly enriched in the macrophage clusters (**Figure 4E**). Furthermore, we found that neutrophils exhibited relatively high chemokine expression in humans (**Figure 4D**). mIHC analysis of human HCC clinical samples also confirmed that CXCL8 was expressed predominantly in macrophages among multiple immune cells (**Figure 4F**). Moreover, CXCL8 expression in $CD68^+$ macrophages was significantly lower in immunotherapy responders than non-responders (**Figure 4G**). Anti-PD-1 antibodies predominantly function on PD-1 expressing cells, so we examined PDCD1 expression among human cell types in the TME. As expected, PD-1/PDCD1 was mainly expressed in T cells at both the protein (**Figure 5A**) and RNA levels (**Figure 5B**). Analyzing the cellular interactions between various cell types showed that macrophages had the strongest interactions with T cells in the TME of HCC (**Figure 5C**). Furthermore, L–R analysis between T cells and macrophages revealed that the IFN-γ-IFNGR pair had a strong interaction, and this interaction was dramatically higher in the post-immunotherapy groups than the pre-immunotherapy groups (**Figure 5C**). Together, these data suggest that anti-PD-1 may indirectly reduce neutrophils *via* the T cell–macrophage axis. This L–R pair has been reported to regulate chemokine secretion by macrophages[36-39].

IFN-γ secreted by anti-PD-1-activated T cell repressed expression of neutrophil-recruiting chemokines by macrophages

To explore whether anti-PD-1 suppresses neutrophil recruitment *via* the T cell (IFN-γ)–macrophage (IFNGR) axis, we co-cultured activated T cells with anti-PD-1 w/o anti-IFN-γ or control in TCM to prime RAW 264.7 macrophages *in vitro*, and the macrophage culture medium was collected for neutrophil migration assays (**Figure 5D**). The macrophage supernatant obtained from co-culture using T cells treated with anti-PD-1 inhibited the migration of neutrophils, which was almost completely rescued by adding anti-IFN-γ, whereas the T cell-only culture medium had no effect on neutrophil migration (**Figure 5E**). To exclude the possibility that neutrophils and cancer cells, which have been reported to express neutrophil-recruiting chemokines, may be involved in neutrophil recruitment, we replaced macrophages with neutrophils or Hepa1-6 cells and repeated the neutrophil migration assay, as described above. Neutrophils (**Figure 5F**) or Hepa1-6 HCC cells (**Figure 5G**) were not responsible for regulating the effect of anti-PD-1 on neutrophil recruitment in this system. The flow cytometry

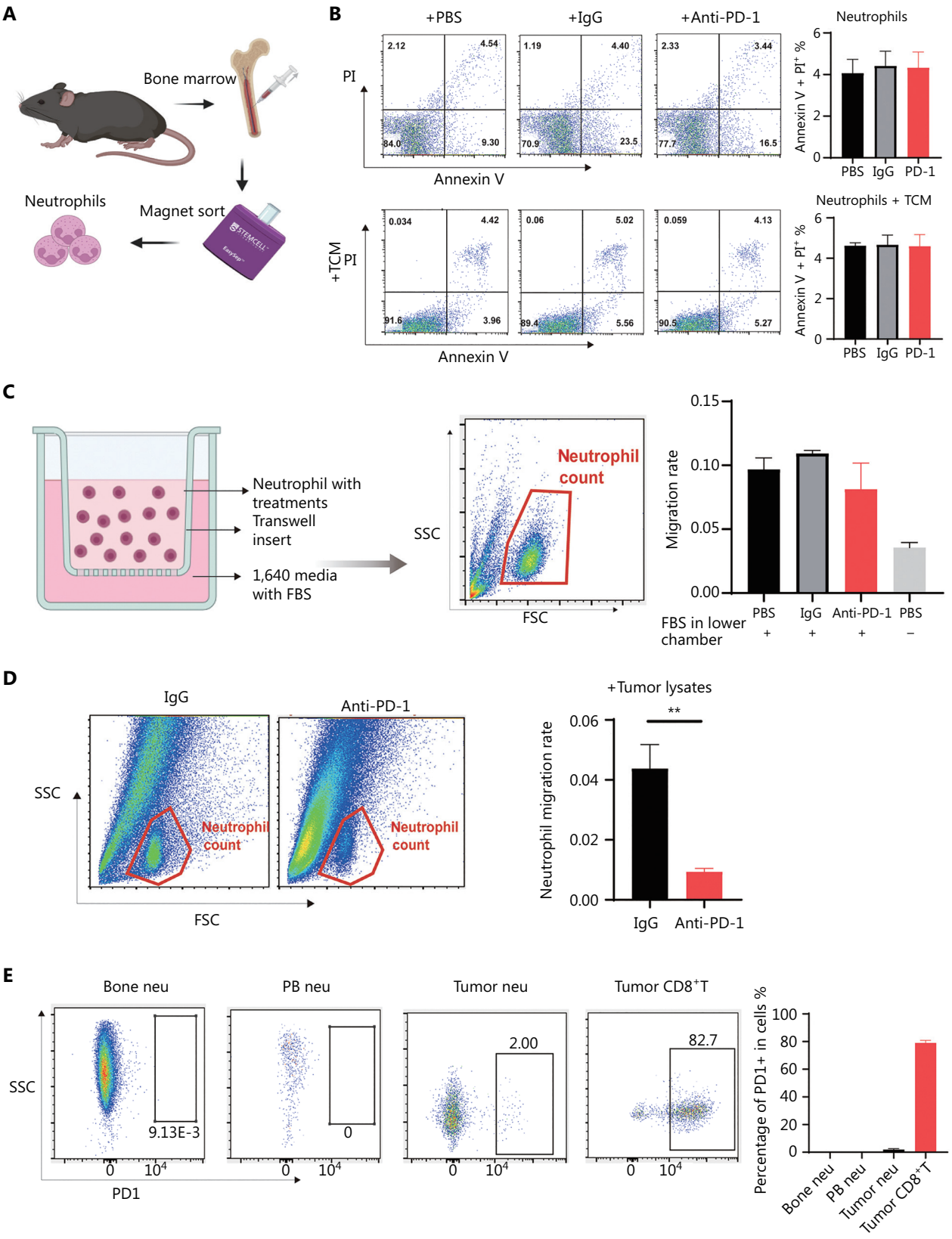

Figure 3 Anti-PD-1 treatment reduced the motility of neutrophils. (A) Schematic diagram showing the isolation of neutrophils from C57BL6/J mice (n = 10). Bone marrows were flushed from femurs and tibiae with sterile PBS. Neutrophils were enriched by magnetic beads selection. (B)

The viability of neutrophils was not affected by anti-PD-1 treatment. Neutrophils pre-incubated with or without Hepa1-6 condition medium were treated with anti-PD-1 or control for Annexin V/PI apoptosis analysis. (C) Schematic showing the Transwell assay. Neutrophils were placed in the upper chamber with the indicated treatments. The lower chamber contained RPMI 1640 medium supplemented with 10% FBS. Migrating cells were determined using flow cytometry. Anti-PD-1 did not influence neutrophil migration *in vitro*, as shown on the right. (D) Anti-PD-1 suppressed the migration ability of neutrophils. Tumor lysates from anti-PD-1 or control-treated groups were diluted 1:1 with RPMI 1640 medium and placed into the lower chamber as a chemoattractant source. The migrated neutrophils were counted and quantified by flow cytometry. $^{**}P < 0.01$, unpaired two-tailed Student's *t*-test. (E) PD-1 was rarely expressed in neutrophils.

counting maps are shown in **Figure S5**. We further validated the expression of chemokines by macrophages under different co-culture conditions and showed that the expression of neutrophil recruitment-related chemokines was reduced in macrophages co-cultured with T cells under anti-PD-1 treatment. This change was rescued by adding anti-IFN-γ (**Figure 5H**). Accumulating evidence has demonstrated that IFN-γ suppresses the secretion of multiple neutrophil-recruiting chemokines by macrophages *via* activation of the JAK-STAT1 pathway[38-40]. Therefore, we examined the expression of classical JAK-STAT1 downstream genes in macrophages. When cocultured with T cells treated with anti-PD-1, macrophages expressed much more *Irf1*, a downstream target gene of JAK-STAT1 signaling, than the control group, and this change was restored by anti-IFN-γ (**Figure 5I**). Syngeneic bone marrow-derived macrophages were used to further validate these observations. Consistent with these results, the phenotypic changes in primary macrophages recapitulated the findings in RAW 264.7 cells (**Figure 5J**). Moreover, the phosphorylation level of STAT1 in primary macrophages, which were co-cultured with active T cells, was higher in the anti-PD-1 treatment group than the controls, and anti-IFN-γ abrogated this upregulation (**Figure 5K**). These results demonstrate that an effective immunotherapy–T cell–macrophage secretion axis controls neutrophil recruitment.

T cell deficient abrogated anti-PD-1 therapy caused reduced neutrophil infiltration

To investigate whether the reduction in neutrophil infiltration following anti-PD-1 treatment depended on the presence or absence of functional T cells, we used nude mice to evaluate the neutrophil dynamics in a T cell-deficient setting under anti-PD-1 treatment. Orthotopic HCC tumors were established in nude mice, followed by treatment with either anti-PD-1 or isotype IgG (**Figure 6A**). The tumor size did not differ significantly between the two treatments (**Figure 6B**). Flow cytometric analysis of the tumors demonstrated that in the absence of T cells, the abundance of neutrophils did not differ significantly between the anti-PD-1 and IgG control groups (**Figure 6C**). Moreover, an *in vitro* chemotaxis migration assay performed to assess neutrophil migration in the absence of T cells under anti-PD-1 therapy revealed that the migration of neutrophils did not differ significantly in the presence of tumor lysates from the anti-PD-1 or IgG groups in the absence of T cells (**Figure 6D**). Consistent with this finding, the ELISA panels obtained using tumor lysates from nude mice did not differ significantly between the anti-PD-1 and isotype control groups (**Figure 6E**). In particular, no substantial alterations in neutrophil recruitment-related chemokines were observed following anti-PD-1 treatment in the absence of mature T cells (**Figure 6F, G**). The standard curves for multiple proteins in ELISA are shown in **Figure S6**.

Discussion

ICB has transformed cancer therapies. However, although the prevailing paradigm has focused on $CD8^+$ T cell reinvigoration, emerging evidence suggests that other immune populations in the TME also play critical roles[41,42]. Clinical observations have shown that a decreased neutrophil-to-lymphocyte ratio is correlated with favorable immunotherapy outcomes[43,44]. A high density of neutrophils in the TME is frequently associated with poor prognosis and resistance to ICI therapies[26], but various alterations occur in neutrophil populations and functions after immunotherapy. An increase in overall neutrophil numbers has historically been linked to negative outcomes, but successful immunotherapy can acutely expand specific tumor neutrophil subsets, particularly those that exhibit a "$Sell^{hi}$ state" in lung cancer mouse models[45].

In this study, we comprehensively investigated the responses of neutrophils to anti-PD-1 immunotherapy by integrating findings from human single-cell transcriptomic analyses, mouse orthotopic HCC models, clinical HCC samples, and *in vitro* mechanistic assays. We found that the neutrophil population decreased in patients with HCC after successful immunotherapy, and elucidated the underlying mechanisms.

Our results obtained from mouse Hepa1-6 allografts generated from C57 immunocompetent mice showed that anti-PD-1 immunotherapy dramatically decreased tumor growth and the TAN population size, confirming our findings in human single-cell transcriptomic analyses. A critical question is whether neutrophils are sensed by anit-PD-1 antibodies directly or indirectly. Myeloid cells can express PD-1 under some conditions, such as inflammation and tumor[46,47]. However, flow

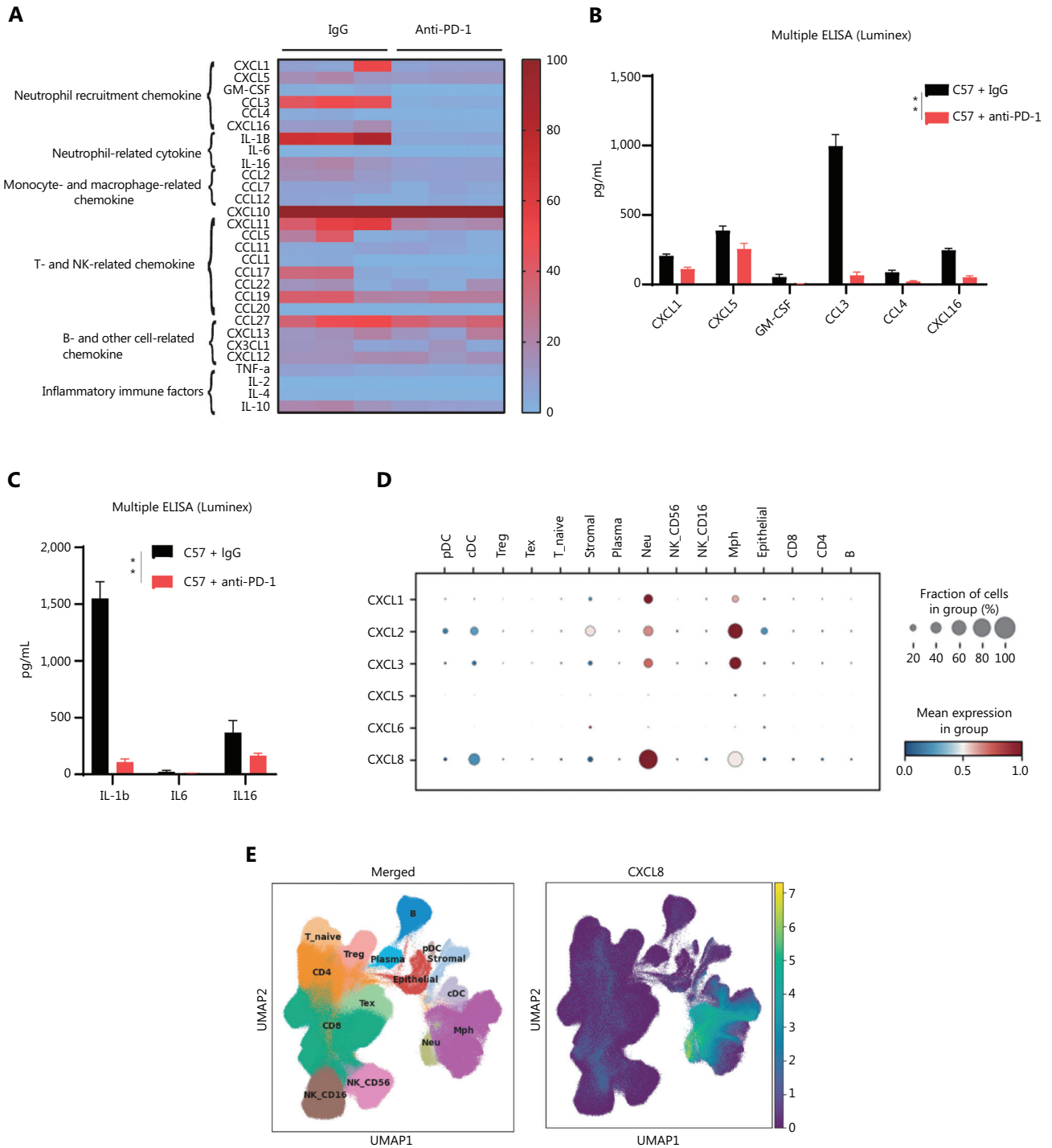

Figure 4 Continued

cytometry analysis of Hepa1-6 allografts showed that PD-1 was only expressed in 2–6% of TANs. *In vitro* assays demonstrated that anti-PD-1 treatment did not affect the migration ability of neutrophils compared with the IgG control, and it did not induce neutrophil apoptosis. Intriguingly, the ICI-resistant H22 tumors exhibited a poor response to anti-PD-1 treatment but also a remarkably high proportion of neutrophils accompanied by markedly scarce T lymphocytes, with no significant differences between the anti-PD-1 and IgG treatment groups. More importantly, anti-PD-1 treatment failed to reduce

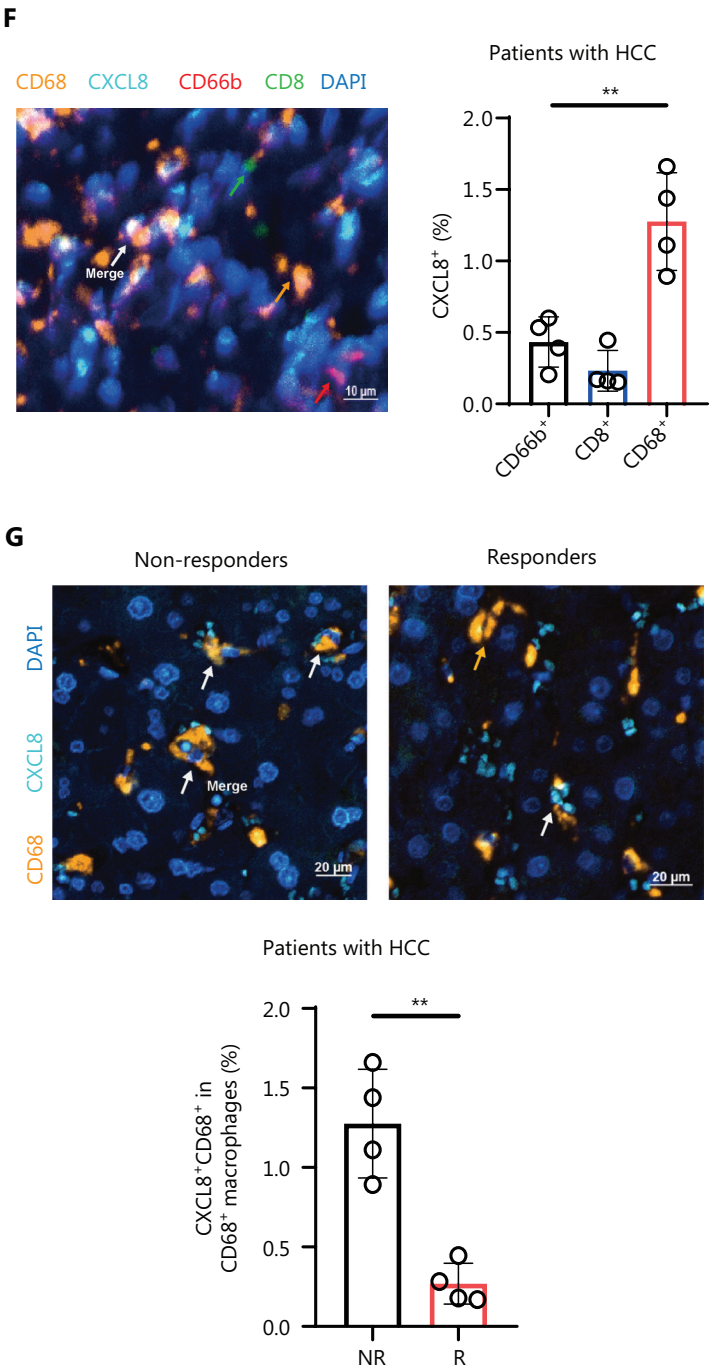

Figure 4 Anti-PD-1 immunotherapy inhibited the expression of neutrophil-recruiting chemokines. (A) Multiple ELISA assay (Luminex) of Hepa1-6 tumors from anti-PD-1 or control treated groups (n = 3 per group). (B) ELISA assay (Luminex) of main neutrophil-recruiting chemokines from anti-PD-1 or control treated tumors. (C) ELISA assay (Luminex) of neutrophil-recruiting cytokines. (D) Comparative analysis of neutrophil chemokine expression levels among major cell types in the TME of HCC patients. (E) UMAP visualization of single cells colored by cell type annotation (left), and feature plot showing CXCL8 expressing areas across the TME (right). (F, G) mIHC staining of human HCC clinical samples, with images analyzed using HALO software (v3.6). Unpaired two-tailed Student's t-test was employed for statistical analysis. $^{**}P$ < 0.01.

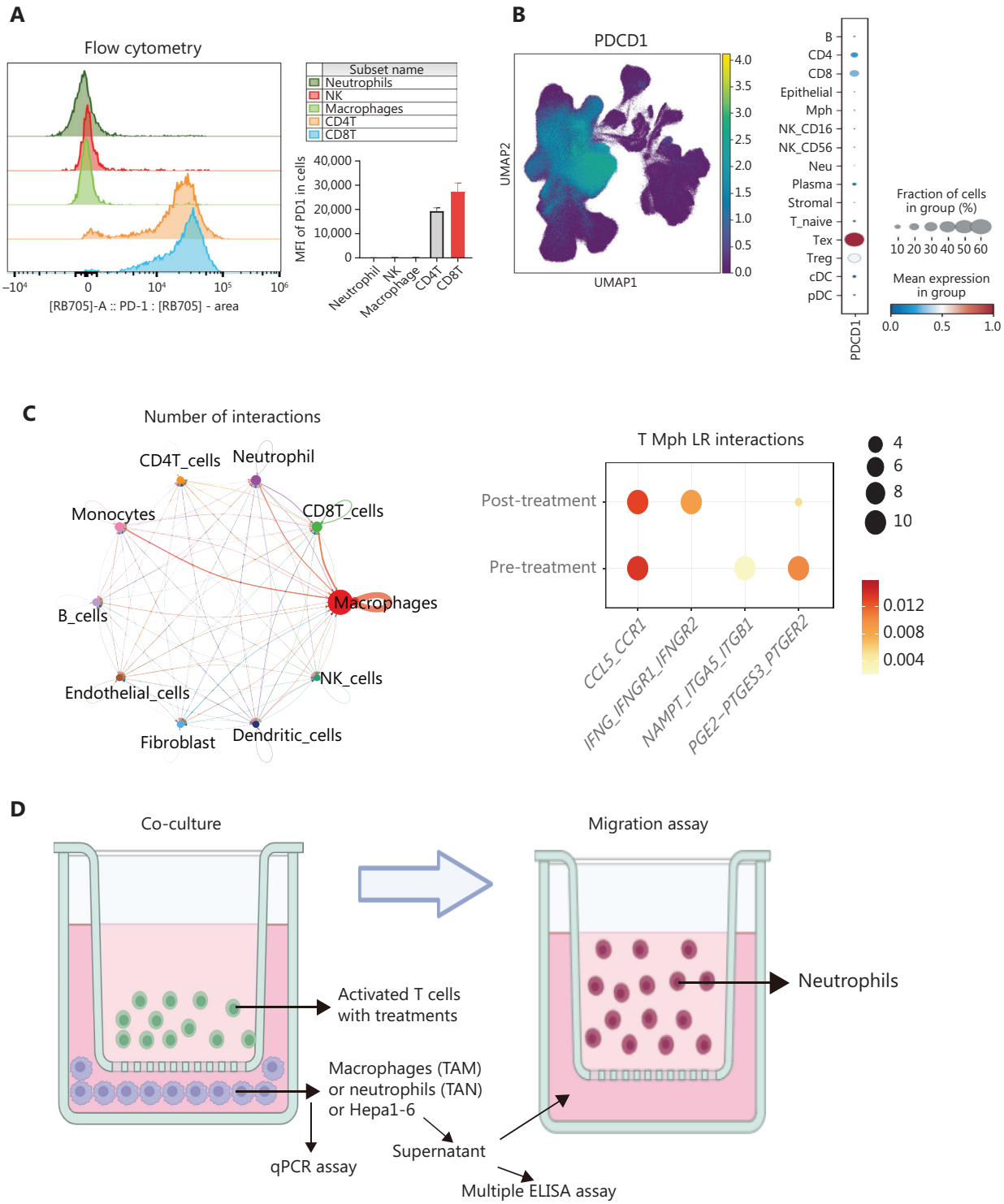

Figure 5 Continued

neutrophil infiltration or alter the chemokine landscape in an immunodeficient HCC allograft mouse model lacking T cells. Thus, we found that neutrophil reduction was indirect and T-cell dependent.

Mechanistically, we identified a T cell–macrophage axis that governs neutrophil recruitment in responding patients and a chemokine axis relay as the key link. The levels of neutrophil recruitment-related chemokines were reduced in the

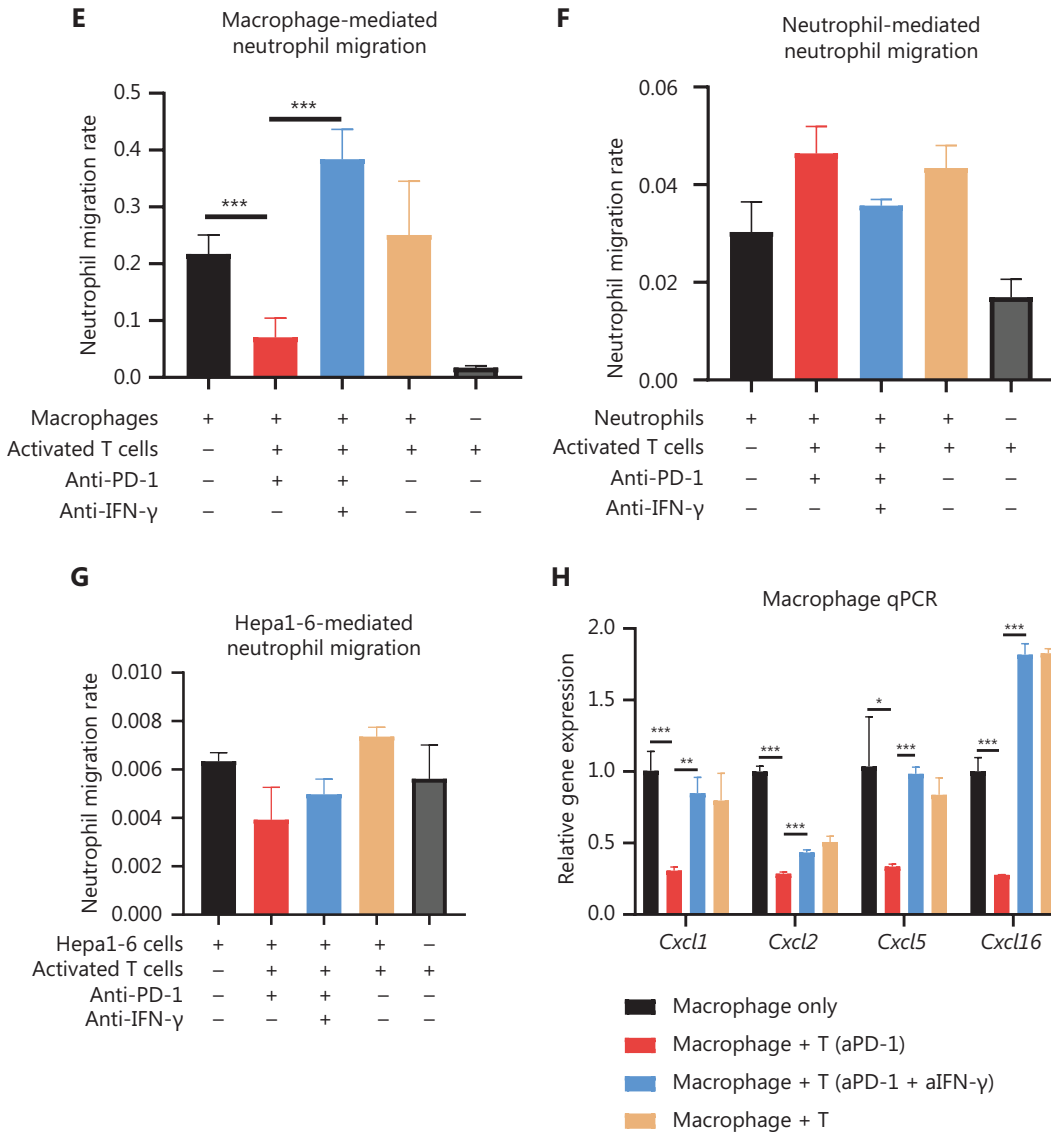

Figure 5 Continued

TME in the anti-PD-1 treatment allograft group. Single-cell analysis of clinical HCC patient samples revealed that TAMs are the primary source of neutrophil chemoattractants, such as CXCL8/1/2/3. This suppression led to reduced chemotaxis by neutrophils in the TME. In addition, data from clinical HCC samples confirmed our findings. As the first line of interaction with anti-PD-1 antibodies, T-cells interact with TAMs, thereby regulating chemokine secretion. Cellular interaction analysis suggested that T cells had strong interactions with TAMs in the TME of HCC, which mainly depended on the IFN-γ/IFNGR L–R pair. Furthermore, it has been demonstrated that IFN-γ suppresses the secretion of neutrophil-related chemokines by macrophages through the JAK-STAT1 pathway[38-40]. Our results showed that both RAW 264.7 macrophages and primary macrophages cocultured with active T cells exhibited enhanced JAK-STAT1 activation when treated with anti-PD-1, which was abrogated by adding anti-IFN-γ. The neutrophil chemotactic capacity of macrophages was also reduced after JAK-STAT1 activation, which repressed the transcription of downstream *Cxcl* chemokine genes. Together, these results indicate that T cells instruct TAMs to reduce the production of neutrophil-related chemokines. Consequently, the accumulation of neutrophils is suppressed in tumors, and the tumor burden is reduced.

Our results revealed that after immunotherapy, the presence of fewer neutrophils in the TME of HCC correlated with a better therapeutic response, suggesting that a low TAN ratio in the TME could be a potential prognostic marker for

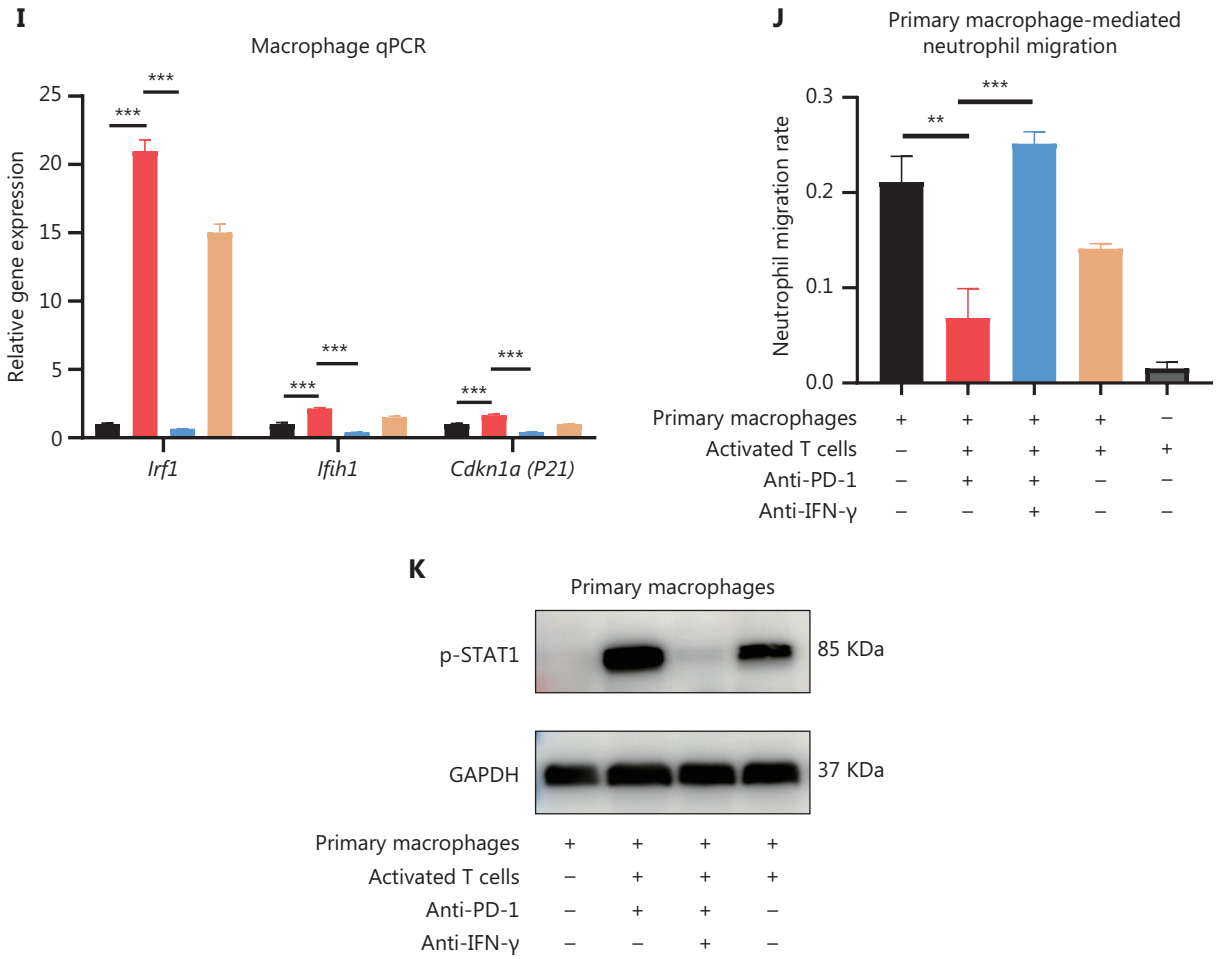

Figure 5 Anti-PD-1 immunotherapy suppressed neutrophil recruitment *via* CD8–TAM axis. (A) PD-1 mainly expressed in T cells in the TME. Representative histogram overlays showing the fluorescence intensity of PD-1 on different cell types, and statistical histogram presenting the mean fluorescence intensity (MFI) in different cell types. (B) UMAP visualization of PDCD1 expression in different cell types in the TME. (C) Cellular interaction analysis between various cell types in the TME. Chord diagram illustrating the strengths of interactions among various cell types (left), and ligand–receptor interaction analysis between T cells and macrophages (right). (D) Schematic showing the experimental workflow. Indicated cells and activated T cells under different treatments were co-cultured for 24 h, before the macrophage supernatant was divided for neutrophil migration assay and multiple ELISA (Luminex) assay. (E) Quantification of neutrophil migration rate with macrophage supernatant from different co-culture media. The migrating neutrophils were detected by flow cytometry. (F) Quantification of neutrophil migration rate with neutrophil supernatant from different co-culture conditions. (G) Quantification of neutrophil migration rate with Hepa1-6 supernatant from different co-culture conditions. (H) qPCR analysis of *Cxcl* gene expression by macrophages under different co-culture conditions. (I) qPCR analysis of classical JAK-STAT1 pathway downstream target gene expression by macrophages under different co-culture conditions. (J) Quantification of neutrophil migration rate with primary macrophage supernatant from different co-culture systems. (K) Western blot of STAT1 phosphorylation in primary macrophages under different conditions. Experiments were performed with three independent biological replicates. Unpaired two-tailed Student's *t*-test, $^{*}P < 0.05$, $^{**}P < 0.01$, $^{***}P < 0.001$.

predicting better outcomes for patients with HCC who have undergone curative surgery following neoadjuvant ICI therapy. Furthermore, the TAN ratio in the TME could be a better indicator than T cells because T cells did not exhibit obvious changes after immunotherapy in some cases[48,49]. In addition, we observed that the abundance of neutrophils was generally lower in responders than non-responders in both pre- and post-immunotherapy statuses. Moreover, the clinical HCC samples from responders exhibited lower neutrophil infiltration compared with those from non-responders (**Figure S1C**). The Human Protein Atlas also showed that a neutrophil marker S100A9 exhibits high expression in HCC and could be a prognostic marker in liver cancer (**Figure S1D**). Subclustering of neutrophils further revealed that responders had

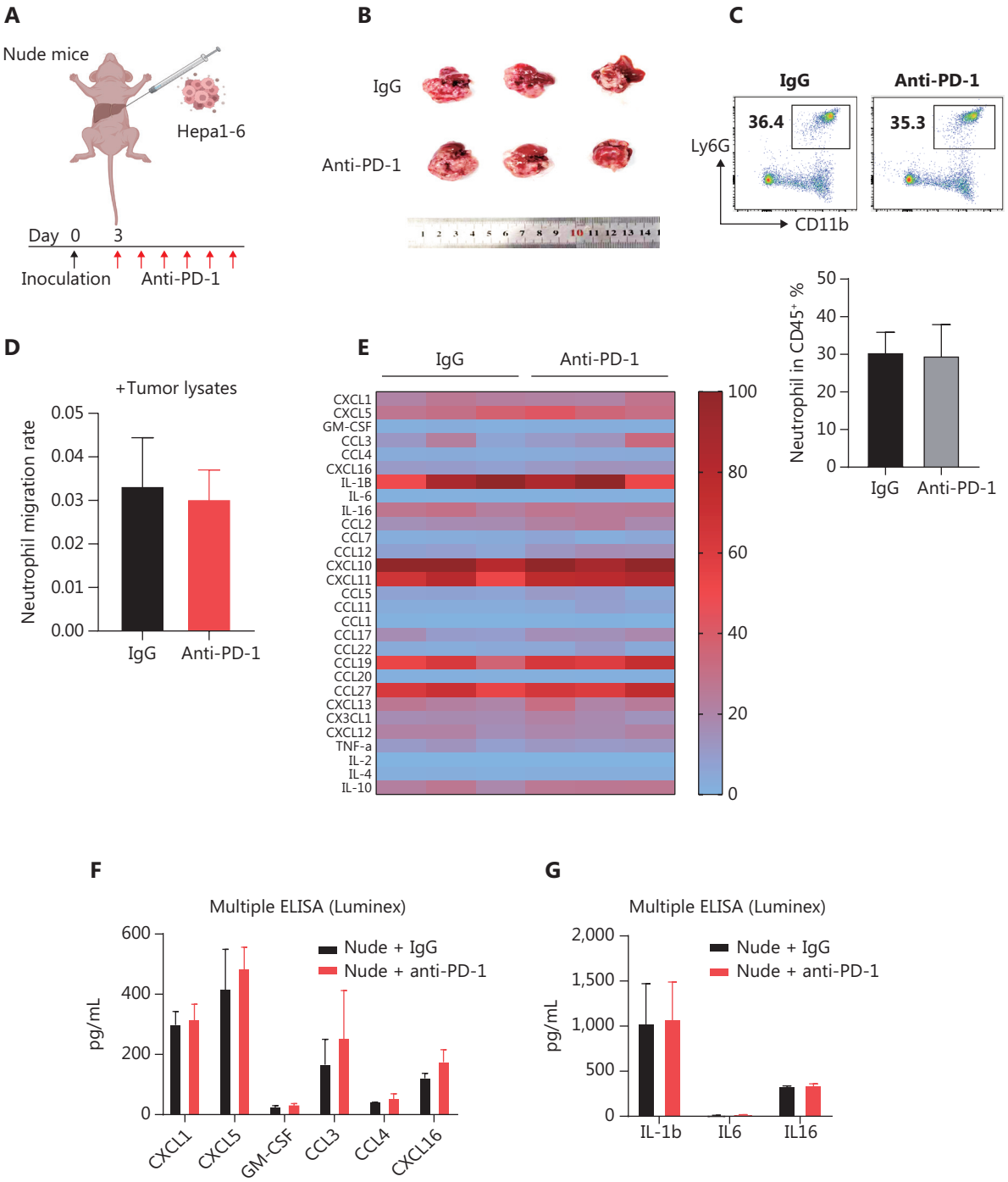

Figure 6 Anti-PD-1 therapy failed to affect neutrophil infiltration under T cell deficiency. (A) Schematic diagram showing the *in vivo* experimental design using nude mice lacking functional T cells (n = 3 per group). (B) Hepa1-6 tumors from nude mice that received anti-PD-1 or isotype control IgG treatment. (C) Flow cytometry analysis of tumor-infiltrating neutrophils. (D) Neutrophil migration assay using tumor lysates from nude mice with different treatments. (E) Multiple ELISA assay (Luminex) of Hepa1-6 tumors from anti-PD-1 or control treated groups (n = 3 per group). (F) Multiple Luminex ELISA assay of main neutrophil-recruiting chemokines from tumors in nude mice from anti-PD-1 or isotype control group. (G) Multiple Luminex ELISA assay of neutrophil-recruiting cytokines.

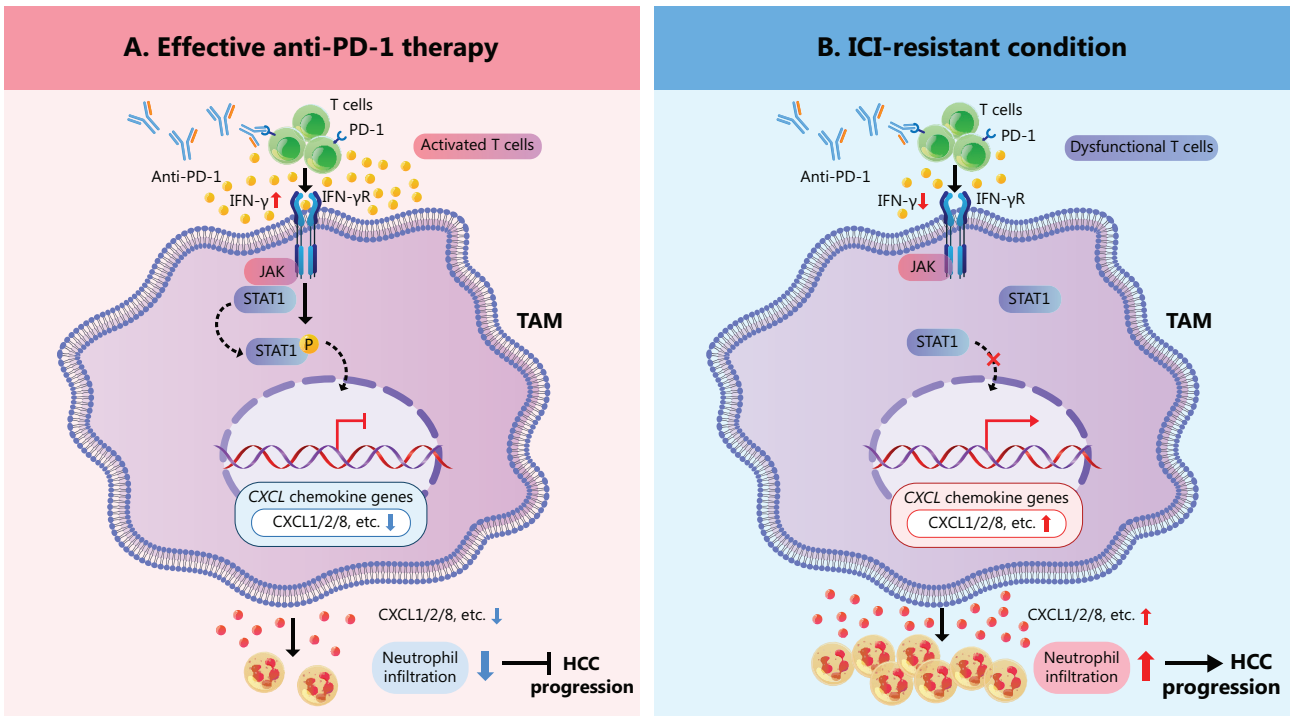

Figure 7 Schematic showing that effective ICI therapy reduces neutrophil infiltration *via* T cell–macrophage chemokine axis. (A) Effective anti-PD-1 therapy enhances IFN-γ secretion by T cells. IFN-γ activates JAK/STAT1 signaling in TAMs, inducing STAT1 phosphorylation and nuclear translocation, which represses transcription of Cxcl chemokine genes in TAMs, thereby reducing the secretion of CXCL chemokines by TAMs. Consequently, the infiltration of neutrophils into the TME is suppressed. (B) Under ICI-resistant conditions, anti-PD-1 therapy fails to trigger substantial IFN-γ release by T cells. JAK/STAT1 signaling in TAMs remains suppressed. Thus, STAT1 remains unphosphorylated and cytoplasmic, allowing the transcription of Cxcl chemokine genes by TAMs to enhance the secretion of CXCL chemokines by TAMs. Consequently, the infiltration of neutrophils into the TME is enhanced. TAMs, tumor-associated macrophages; TME, tumor microenvironment; ICI, immune checkpoint inhibitor; IFN-γ, interferon-gamma; IFN-γR, interferon-gamma receptor; JAK, Janus kinase; STAT1, signal transducer and activator of transcription 1; p-STAT1, phosphorylated-STAT1; CXCL, C-X-C motif chemokine ligand. Figure created using BioRender (www.biorender.com) and Adobe Illustrator.

more favorable N1-like neutrophil subsets, whereas N2-lile neutrophils predominated in non-responders[50] (**Figure S1E–G**). A limitation of this study is that data for 104 samples from only 46 patients with HCC were included in this study, and a larger cohort with neutrophil quantification data and prognosis information will help to further strengthen our findings in the future.

In conclusion, our results demonstrate that neutrophil infiltration was significantly reduced after effective immunotherapy. We identified a previously unrecognized T cell–TAM–neutrophil communication axis in the TME that was altered by anti-PD-1 treatment, leading to reduced recruitment of neutrophils. (**Figure 7**) More broadly, these findings show that the success of immunotherapy depends on T-cell reinvigoration, but also on remodeling of the entire immune system, especially myeloid cells. Importantly, the change in neutrophil infiltration could serve a critical role in monitoring the immunotherapy process and compensate for changes in T cells. As clinical approaches move toward combination therapies, targeting the T cell–TAMs axis may provide new opportunities for overcoming immunotherapy resistance and enhancing clinical outcomes.

Acknowledgments

We thank the Department of Laboratory Animal Science and the Core Facility Management Platform of the Peking University Health Science Center.

Grant support

This study was jointly supported by the National Natural Science Foundation of China (Grant Nos. 82588201, 82030079, and 82341005 to NZ, and Grant No. 82073270 to

RL), National Key R&D Program of China (NKRDPC) (Grant No. 2022YFC3400901 to NZ), and Beijing Natural Science Foundation (Grant No. L2510036 to RL).

Conflict of interest statement

No potential conflicts of interest are disclosed.

Author contributions

Conceived and designed the analysis: Rong Liu, Ning Zhang, Jiahao Huang.
Collected the data: Jiahao Huang, Boyang Yi, Kuo Qi, Delin Ma, Feifei Sun, Bo Han.
Contributed data or analysis tools: Jiahao Huang, Boyang Yi, Yijie Zhao, Wuzhou Wan.
Performed the analysis: Jiahao Huang.
Wrote the paper: Jiahao Huang, Rong Liu.

Data availability statement

The data generated in this study are publicly available in Gene Expression Omnibus (GEO) with accession numbers GSE235863 and GSE206325, and the Genome Sequence Archive in the National Genomics Data Center *via* number HRA007658 and Mendeley Data (skrx2fz79n). The data generated in this study are available upon request from the corresponding author.

References

1. Singal AG, Kanwal F, Llovet JM. Global trends in hepatocellular carcinoma epidemiology: implications for screening, prevention and therapy. Nat Rev Clin Oncol. 2023; 20: 864-84.
2. Huang DQ, Singal AG, Kanwal F, Lampertico P, Buti M, Sirlin CB, et al. Hepatocellular carcinoma surveillance – utilization, barriers and the impact of changing aetiology. Nat Rev Gastroenterol Hepatol. 2023; 20: 797-809.
3. Mak LY, Liu K, Chirapongsathorn S, Yew KC, Tamaki N, Rajaram RB, et al. Liver diseases and hepatocellular carcinoma in the Asia-Pacific region: burden, trends, challenges and future directions. Nat Rev Gastroenterol Hepatol. 2024; 21: 834-51.
4. Yang C, Zhang H, Zhang L, Zhu AX, Bernards R, Qin W, et al. Evolving therapeutic landscape of advanced hepatocellular carcinoma. Nat Rev Gastroenterol Hepatol. 2023; 20: 203-22.
5. Yau T, Galle PR, Decaens T, Sangro B, Qin S, da Fonseca LG, et al. Nivolumab plus ipilimumab versus lenvatinib or sorafenib as first-line treatment for unresectable hepatocellular carcinoma (CheckMate 9DW): an open-label, randomised, phase 3 trial. Lancet. 2025; 405: 1851-64.
6. Llovet JM, Castet F, Heikenwalder M, Maini MK, Mazzaferro V, Pinato DJ, et al. Immunotherapies for hepatocellular carcinoma. Nat Rev Clin Oncol. 2022; 19: 151-72.
7. Zheng J, Wang S, Xia L, Sun Z, Chan KM, Bernards R, et al. Hepatocellular carcinoma: signaling pathways and therapeutic advances. Signal Transduct Target Ther. 2025; 10: 35.
8. Ma L, Hernandez MO, Zhao Y, Mehta M, Tran B, Kelly M, et al. Tumor cell biodiversity drives microenvironmental reprogramming in liver cancer. Cancer Cell. 2019; 36: 418-30.e6.
9. Sharma P, Goswami S, Raychaudhuri D, Siddiqui BA, Singh P, Nagarajan A, et al. Immune checkpoint therapy-current perspectives and future directions. Cell. 2023; 186: 1652-69.
10. Latchman Y, Wood CR, Chernova T, Chaudhary D, Borde M, Chernova I, et al. PD-L2 is a second ligand for PD-1 and inhibits T cell activation. Nat Immunol. 2001; 2: 261-8.
11. Sun Q, Hong Z, Zhang C, Wang L, Han Z, Ma D. Immune checkpoint therapy for solid tumours: clinical dilemmas and future trends. Signal Transduct Target Ther. 2023; 8: 320.
12. Boussiotis VA. Molecular and biochemical aspects of the PD-1 checkpoint pathway. N Engl J Med. 2016; 375: 1767-78.
13. Sun C, Mezzadra R, Schumacher TN. Regulation and function of the PD-L1 checkpoint. Immunity. 2018; 48: 434-52.
14. Pérez-Ruiz E, Melero I, Kopecka J, Sarmento-Ribeiro AB, García-Aranda M, De Las Rivas J. Cancer immunotherapy resistance based on immune checkpoints inhibitors: targets, biomarkers, and remedies. Drug Resist Updat. 2020; 53: 100718.
15. Gu L, Peng C, Liang Q, Huang Q, Lv D, Zhao H, et al. Neoadjuvant toripalimab plus axitinib for clear cell renal cell carcinoma with inferior vena cava tumor thrombus: NEOTAX, a phase 2 study. Signal Transduct Target Ther. 2024; 9: 264.
16. Mishra R, Sukhbaatar A, Mori S, Kodama T. Metastatic lymph node targeted CTLA4 blockade: a potent intervention for local and distant metastases with minimal ICI-induced pneumonia. J Exp Clin Cancer Res. 2023; 42: 132.
17. Nicolas-Avila JA, Adrover JM, Hidalgo A. Neutrophils in homeostasis, immunity, and cancer. Immunity. 2017; 46: 15-28.
18. Ng LG, Ostuni R, Hidalgo A. Heterogeneity of neutrophils. Nat Rev Immunol. 2019; 19: 255-65.
19. Geh D, Leslie J, Rumney R, Reeves HL, Bird TG, Mann DA. Neutrophils as potential therapeutic targets in hepatocellular carcinoma. Nat Rev Gastroenterol Hepatol. 2022; 19: 257-73.
20. Marteau V, Nemati N, Handler K, Raju D, Kirchmair A, Rieder D, et al. Single-cell integration and multi-modal profiling reveals phenotypes and spatial organization of neutrophils in colorectal cancer. Cancer Cell. 2026; 44: 146-65.e14.
21. Guo W, Luan J, Huang X, Leon D, Gang S, Nicholson B, et al. Tumor-initiating stem cells fine-tune the plasticity of neutrophils to sculpt a protective niche. Cancer Cell. 2026; 44: 94-111.e11.
22. Xue R, Zhang Q, Cao Q, Kong R, Xiang X, Liu H, et al. Liver tumour immune microenvironment subtypes and neutrophil heterogeneity. Nature. 2022; 612: 141-7.
23. Wu Y, Ma J, Yang X, Nan F, Zhang T, Ji S, et al. Neutrophil profiling illuminates anti-tumor antigen-presenting potency. Cell. 2024; 187: 1422-39.e24.

24. Ng MSF, Kwok I, Tan L, Shi C, Cerezo-Wallis D, Tan Y, et al. Deterministic reprogramming of neutrophils within tumors. Science. 2024; 383: eadf6493.
25. Maas RR, Soukup K, Fournier N, Massara M, Galland S, Kornete M, et al. The local microenvironment drives activation of neutrophils in human brain tumors. Cell. 2023; 186: 4546-66.e27.
26. Zhang H, Houghton AM. Good cops turn bad: the contribution of neutrophils to immune-checkpoint inhibitor treatment failures in cancer. Pharmacol Ther. 2021; 217: 107662.
27. Cupp MA, Cariolou M, Tzoulaki I, Aune D, Evangelou E, Berlanga-Taylor AJ. Neutrophil to lymphocyte ratio and cancer prognosis: an umbrella review of systematic reviews and meta-analyses of observational studies. BMC Med. 2020; 18: 360.
28. Li T, Guo S, Xu C, Zhang M, Lyu C, Xu H, et al. Integrated single-cell transcriptome and TCR profiles of hepatocellular carcinoma highlight the convergence on interferon signaling during immunotherapy. J Immunother Cancer. 2024; 12: e010534.
29. Guo X, Nie H, Zhang W, Li J, Ge J, Xie B, et al. Contrasting cytotoxic and regulatory T cell responses underlying distinct clinical outcomes to anti-PD-1 plus lenvatinib therapy in cancer. Cancer Cell. 2025; 43: 248-68.e9.
30. Magen A, Hamon P, Fiaschi N, Soong BY, Park MD, Mattiuz R, et al. Intratumoral dendritic cell-CD4$^+$ T helper cell niches enable CD8$^+$ T cell differentiation following PD-1 blockade in hepatocellular carcinoma. Nat Med. 2023; 29: 1389-99.
31. Liu Y, Xun Z, Ma K, Liang S, Li X, Zhou S, et al. Identification of a tumour immune barrier in the HCC microenvironment that determines the efficacy of immunotherapy. J Hepatol. 2023; 78: 770-82.
32. Wolf FA, Angerer P, Theis FJ. SCANPY: large-scale single-cell gene expression data analysis. Genome Biol. 2018; 19: 15.
33. Chen H, Li Z, Qiu L, Dong X, Chen G, Shi Y, et al. Personalized neoantigen vaccine combined with PD-1 blockade increases CD8$^+$ tissue-resident memory T-cell infiltration in preclinical hepatocellular carcinoma models. J Immunother Cancer. 2022; 10: e004389.
34. Caronni N, La Terza F, Frosio L, Ostuni R. IL-1β$^+$ macrophages and the control of pathogenic inflammation in cancer. Trends Immunol. 2025; 46: 403-15.
35. Radharani NNV, Yadav AS, Nimma R, Kumar TVS, Bulbule A, Chanukuppa V, et al. Tumor-associated macrophage derived IL-6 enriches cancer stem cell population and promotes breast tumor progression via Stat-3 pathway. Cancer Cell Int. 2022; 22: 122.
36. Hodge-Dufour J, Marino MW, Horton MR, Jungbluth A, Burdick MD, Strieter RM, et al. Inhibition of interferon γ induced interleukin 12 production: a potential mechanism for the anti-inflammatory activities of tumor necrosis factor. Proc Natl Acad Sci U S A. 1998; 95: 13806-11.
37. Deng W, Ohmori Y, Hamilton TA. Mechanisms of IL-4-mediated suppression of IP-10 gene expression in murine macrophages. J Immunol. 1994; 153: 2130-6.
38. Hoeksema MA, Scicluna BP, Boshuizen MCS, van der Velden S, Neele AE, Van den Bossche J, et al. IFN-γ priming of macrophages represses a part of the inflammatory program and attenuates neutrophil recruitment. J Immunol. 2015; 194: 3909-16.
39. Stock AT, Smith JM, Carbone FR. Type I IFN suppresses Cxcr2 driven neutrophil recruitment into the sensory ganglia during viral infection. J Exp Med. 2014; 211: 751-9.
40. Boroujeni ME, Lopacinska N, Antonczyk A, Kluzek K, Wesoly J, Bluyssen HAR. Integrative multi-omics analysis of IFNγ-induced macrophages and atherosclerotic plaques reveals macrophage-dependent STAT1-driven transcription in atherosclerosis. Front Immunol. 2025; 16: 1590953.
41. Bader JE, Wolf MM, Lupica-Tondo GL, Madden MZ, Reinfeld BI, Arner EN, et al. Obesity induces PD-1 on macrophages to suppress anti-tumour immunity. Nature. 2024; 631: E16.
42. Tay C, Tanaka A, Sakaguchi S. Tumor-infiltrating regulatory T cells as targets of cancer immunotherapy. Cancer Cell. 2023; 41: 450-65.
43. Hwang M, Canzoniero JV, Rosner S, Zhang G, White JR, Belcaid Z, et al. Peripheral blood immune cell dynamics reflect antitumor immune responses and predict clinical response to immunotherapy. J Immunother Cancer. 2022; 10: e004688.
44. Templeton AJ, McNamara MG, Šeruga B, Vera-Badillo FE, Aneja P, Ocaña A, et al. Prognostic role of neutrophil-to-lymphocyte ratio in solid tumors: a systematic review and meta-analysis. J Natl Cancer Inst. 2014; 106: dju124.
45. Gungabeesoon J, Gort-Freitas NA, Kiss M, Bolli E, Messemaker M, Siwicki M, et al. A neutrophil response linked to tumor control in immunotherapy. Cell. 2023; 186: 1448.
46. Chamoto K, Yaguchi T, Tajima M, Honjo T. Insights from a 30-year journey: function, regulation and therapeutic modulation of PD1. Nat Rev Immunol. 2023; 23: 682-95.
47. Strauss L, Mahmoud MAA, Weaver JD, Tijaro-Ovalle NM, Christofides A, Wang Q, et al. Targeted deletion of PD-1 in myeloid cells induces antitumor immunity. Sci Immunol. 2020; 5: eaay1863.
48. Friedrich MJ, Raab MS. When the silence speaks: T-cell dysfunction in myeloma. Blood. 2025; 145: 3064-6.
49. Khojandi N, Connelly L, Piening A, Hoft SG, Pherson M, Donlin MJ, et al. Single-cell analysis of peripheral CD8$^+$ T cell responses in patients receiving checkpoint blockade immunotherapy for cancer. Cancer Immunol Immunother. 2023; 72: 397-408.
50. Fridlender ZG, Sun J, Kim S, Kapoor V, Cheng G, Ling L, et al. Polarization of tumor-associated neutrophil phenotype by TGF-β: "N1" versus "N2" TAN. Cancer Cell. 2009; 16: 183-94.

Cite this article as: Huang J, Yi B, Qi K, Ma D, Sun F, Han B, et al. Effective anti-PD-1 therapy reduces neutrophil infiltration *via* T cell–macrophage chemokine axis in hepatocellular carcinoma. Cancer Biol Med. 2026; x: xx-xx. doi: 10.20892/j.issn.2095-3941.2026.0468